

Can exact scaling exponents be obtained using the renormalization group? Affirmative evidence from incompressible polar active fluids

Patrick Jentsch* and Chiu Fan Lee†
Department of Bioengineering, Imperial College London,
South Kensington Campus, London SW7 2AZ, U.K.

(Dated: April 19, 2024)

In active matter systems, non-Gaussian, exact scaling exponents have been claimed in a range of systems using perturbative renormalization group (RG) methods. This is unusual compared to equilibrium systems where non-Gaussian exponents can typically only be approximated, even using the exact (or functional/nonperturbative) renormalization group (ERG). Here, we perform an ERG analysis on the ordered phase of incompressible polar active fluids and find that the *exact* non-Gaussian exponents obtained previously using a perturbative RG method remain valid even in this nonperturbative setting. Furthermore, our ERG analysis elucidates the RG flow of this system and enables us to identify an active Goldstone regime with nontrivial, long-ranged scaling behavior for parallel and longitudinal fluctuations.

Renormalization group (RG) methodology constituted one of the greatest advances in the toolbox of theoretical physicists in the past 50 years and has brought many great advances in physics since its inception. Originated from particle and condensed matter physics [1–6], RG techniques have since found applications in diverse disciplines of physics. In the context of many-body physics, RG methods enable us to identify emergent behavior that is *universal* to a wide class of systems sharing the same key qualitative characteristics features, such as the underlying conservation laws and symmetries [7, 8]. Furthermore, RG provides us with a way to classify many-body systems into distinct *universality classes* (UCs), each of which is associated with a unique RG fixed point. Importantly, distinct UCs typically exhibit quantitatively different scale-invariant structures and thus leave measurable experimental imprints.

Interestingly, this also provides a way to ascertain novelty in physics: a system can be said to exhibit novel physics if it is governed by a novel UC. In this regard, the nascent field of active matter, nonequilibrium many-body systems that generate local stresses at the constituent-level [9, 10], has been a treasure trove of novel UCs: diverse new critical phenomena and nonequilibrium phases have been uncovered in the recent past (see [11–19] for recent examples).

However, while the novelty of these dynamical systems can typically be identified through analytical RG calculations, the accompanying quantitative features can be more difficult to discern. This is partly because RG calculations have historically been perturbative in nature, with the ϵ -expansion method being one of the most popular methods used [20, 21]. In an ϵ -expansion, the supposed “small” parameter ϵ corresponds to the value between the spatial dimension of interest and a model-dependent upper critical dimension, d_u . Unfortunately, d_u is for many systems beyond any physical dimensions (e.g., $d_u = 4$ for the critical Ising model), thus making a quantitative RG calculation using the ϵ -expansion

method in physical dimensions, where $\epsilon = 1$ or $\epsilon = 2$, questionable.

Undeterred, physicists continued to make great strides in developing RG methodology. In particular, tremendous advances have been made in exact (or functional/nonperturbative) RG methods [22–24], which was shown to be quantitatively accurate when applied to diverse physical systems [25]. Despite the namesake, practitioners of exact RG (ERG) calculations almost never claim that their outputs, such as the scaling exponents computed, are actually *exact* when dealing with a nontrivial RG fixed point. This is because an ERG calculation is invariably coupled to an approximation scheme, such as the derivative expansion [26–29] or the BMW approximation [30–32]. The accuracy of scaling exponents obtained in such an approximation can typically be improved, by incorporating higher-order terms which are irrelevant by naive power-counting. For example, the convergence of the derivative expansion to the virtually exact exponents has been demonstrated quantitatively for the critical point of $O(N)$ models [28, 29].

Since in general it is impossible to perform an ERG calculation on a completely generic Hamiltonian (i.e., with infinitely many terms), no exact results can be expected. Ironically, practitioners of the perturbative dynamic RG (DRG) [33] have long claimed that they have found numerically exact scaling exponents across a spectrum of dimensions in biology-inspired systems [12, 34–38]. So how can both observations be reconciled?

In this Letter, we provide strong evidence that for some systems exact calculations can be performed using RG methods. Specifically, we apply ERG to analyze the ordered phase of incompressible polar active fluids (IPAF) in three dimensions, whose associated scaling exponents were claimed to be determined exactly using the perturbative DRG method [36].

By performing an ERG calculation on the same system from scratch, we confirm the existence of the fixed point, which previously was only assumed, and find that

the scaling exponents [36] remain unchanged, thus affirming the *exact* nature of these quantities. Further, we find an *active Goldstone regime*, where two other modes: velocity fluctuations that are aligned with collective motion and wavevector respectively, become soft and exhibit nontrivial scaling behavior.

In the following, we will first recapitulate the key arguments in the DRG calculation in Ref. [36] that lead to the claim of exact scaling exponents. We then reanalyze IPAF using out-of-equilibrium ERG [39] with a more general ansatz, and show that the scaling exponents remain unmodified. In the course of the analysis, we will find a more general fixed point than described before, realizing the active Goldstone regime.

A recap of DRG on IPAF.—The equation of motion (EOM) that governs generic IPAF corresponds to the incompressible version of the Toner-Tu EOM for generic compressible polar active fluids. Specifically, denoting the system's velocity field by \mathbf{v} , the EOM is

$$\partial_t \mathbf{v} + \lambda(\mathbf{v} \cdot \nabla) \mathbf{v} = -\nabla \mathcal{P} - (a + b|\mathbf{v}|^2) \mathbf{v} + \mu \nabla^2 \mathbf{v} + \text{h.o.t.} + \mathbf{f}, \quad (1)$$

where \mathcal{P} is the “pressure” term (or Lagrange multiplier) present to enforce the incompressibility condition $\nabla \cdot \mathbf{v} = 0$ and “h.o.t.” denotes *higher order terms*, i.e., terms of higher order in both \mathbf{v} and the spatial derivatives. Finally, \mathbf{f} is a zero-mean Gaussian noise with statistics:

$$\langle f_m(\mathbf{r}, t) f_n(\mathbf{r}', t') \rangle = 2D \delta^d(\mathbf{r} + \mathbf{r}') \delta(t + t'). \quad (2)$$

Since in the ordered phase the continuous rotational symmetry is broken spontaneously, we expect that the resulting Goldstone modes exhibit scaling behavior that is described by a RG fixed point. Specifically, letting $\mathbf{u} = \mathbf{v} - |\langle \mathbf{v} \rangle| \hat{\mathbf{x}}$ where $\hat{\mathbf{x}}$ denotes, without loss of generality, the direction of the collective motion $\langle \mathbf{v} \rangle$, we expect that

$$\langle \mathbf{u}_\perp(\mathbf{0}, 0) \cdot \mathbf{u}_\perp(\mathbf{r}, t) \rangle = |\mathbf{r}_\perp|^{2\chi} S \left(\frac{x - \nu t}{|\mathbf{r}_\perp|^\zeta}, \frac{t}{|\mathbf{r}_\perp|^z} \right), \quad (3)$$

where “ \perp ” denotes components perpendicular to $\hat{\mathbf{x}}$ and so \mathbf{u}_\perp corresponds to the Goldstone modes in the ordered phase. Furthermore, S in Eq. (3) is a scaling function that is universal up to a model-dependent constant prefactor, and ν is again a model-dependent constant.

Using a DRG analysis, it is claimed in Ref. [36] that in $2 < d \leq 4$, the values of the scaling exponents are *exactly* given by

$$\chi = \frac{3 - 2d}{5}, \quad \zeta = \frac{d + 1}{5}, \quad z = \frac{2(d + 1)}{5}. \quad (4)$$

We now summarize the chain of arguments leading to the claim of exact scaling exponents that describe the ordered phase of IPAF.

Step 1. An analysis of the linearized version of the EOM (1) indicates that the correlation function $\langle \mathbf{u}(\mathbf{k}, t) \cdot$

$\mathbf{u}(\mathbf{k}', t') \rangle$ is dominated by $\langle \mathbf{u}_T(\mathbf{k}, t) \cdot \mathbf{u}_T(\mathbf{k}', t') \rangle$ where $\mathbf{u}_T(\mathbf{k}, t) \equiv \mathbf{u}_\perp(\mathbf{k}, t) - [\mathbf{u}_\perp(\mathbf{k}, t) \cdot \hat{\mathbf{k}}] \hat{\mathbf{k}}$.

Step 2. After determining the dominant components in the fluctuations, the most dominant nonlinear terms in the EOM are identified by power counting. Retaining only the most relevant nonlinear term, the reduced EOM of \mathbf{u}_\perp , in the comoving frame along $\hat{\mathbf{x}}$, is found to be

$$\partial_t \mathbf{u}_\perp + \lambda(\mathbf{u}_\perp \cdot \nabla_\perp) \mathbf{u}_\perp = -\nabla_\perp \mathcal{P} + \mu_\perp \nabla_\perp^2 \mathbf{u}_\perp + \mu_x \partial_x^2 \mathbf{u}_\perp + \mathbf{f}_\perp. \quad (5)$$

In particular, the upper critical dimension d_u is 4.

Step 3. The RG flow equations of the four model coefficients ($\lambda, \mu_\perp, \mu_x$ and D) evaluated at the fixed point (that is assumed to exist) lead to four linear algebraic equations in terms of the yet to be determined scaling exponents χ, ζ , and z , and potential graphical corrections. However, since the structure of the EOM corresponds exactly to the model equation analyzed by Toner and Tu in 1995 [35], we know that only one of the coefficients (μ_\perp) admits a graphical correction (G_{μ_\perp}). The four linear equations obtained at the RG fixed point thus enable us to solve for the four unknowns: χ, ζ, z and G_{μ_\perp} , using simple linear algebra, yielding Eq. (4).

Step 4. One can now use the scaling exponents obtained to check that all other nonlinear terms ignored in the analysis remain irrelevant for $d = 3$. Therefore, the scaling behavior of the system is claimed to be described by the exact scaling exponents obtained.

ERG on IPAF.—We now reanalyze the ordered phase of IPAF from scratch to answer the questions: Does the fixed point actually exist? And can nonperturbative effects modify the scaling behavior (4)? Akin to the treatment of passive incompressible fluids with long-ranged forcing, described by the Navier-Stokes equation [41, 42], we first convert the EOM (1) to an action using the Martin-Siggia-Rose-De Dominicis-Janssen formalism [43–45], keeping the pressure as an auxiliary variable that enforces the incompressibility condition,

$$S[\bar{\mathbf{v}}, \mathbf{v}, \bar{\mathcal{P}}, \mathcal{P}] = \int_{\bar{\mathbf{r}}} \left\{ \bar{\mathbf{v}} \cdot \left[\partial_t \mathbf{v} + \lambda(\mathbf{v} \cdot \nabla) \mathbf{v} + \nabla \mathcal{P} - \mu \nabla^2 \mathbf{v} + (a + b|\mathbf{v}|^2) \mathbf{v} \right] - D|\bar{\mathbf{v}}|^2 + \bar{\mathcal{P}} \nabla \cdot \mathbf{v} \right\}, \quad (6)$$

where $\int_{\bar{\mathbf{r}}} = \int d^d \mathbf{r} dt$ and $\bar{\mathbf{v}}$ and $\bar{\mathcal{P}}$ are the response fields introduced by the formalism.

Expressed in this form, the functional renormalization group formalism, based on the exact Wetterich equation [22–24],

$$\partial_k \Gamma_k = \frac{1}{2} \text{Tr} \left[\left(\Gamma_k^{(2)} + R_k \right)^{-1} \partial_k R_k \right], \quad (7)$$

where the trace Tr sums over all degrees of freedom, i.e., field indices, wavenumbers, and frequencies, can now straightforwardly be applied. Eq. (7) describes the

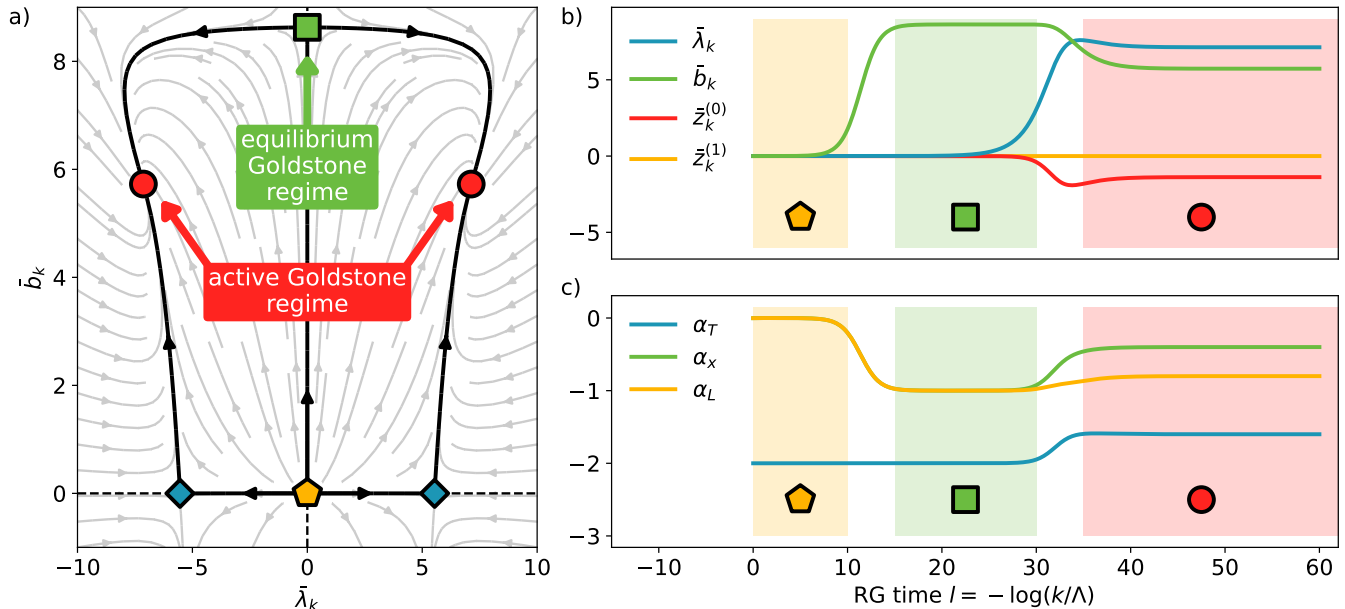


FIG. 1. a) Two-dimensional projection of the RG flow diagram in $d = 3$ (how the projection is obtained is explained in Ref. [40]). The yellow pentagon denotes the trivial Gaussian fixed point and the blue diamond the universality class described in [36]. At the green square, the system is in the Goldstone regime of the equilibrium $O(N)$ model (for $N = d - 1$). Finally the red circle denotes the active Goldstone regime described in this paper. b) A specific RG trajectory in $d = 3$ which shows a crossover from the Gaussian fixed point (yellow pentagon) over the equilibrium Goldstone regime (green square) to the active Goldstone regime (red circle). c) The scaling dimension of the 3 different dynamical modes along the same trajectory as in b). In the active Goldstone regime the Goldstone modes scaling dimension, α_T , agrees with the value calculated in Ref. [36], while the other two modes not considered in Ref. [36], α_T and α_L , show novel scaling behavior.

coarse-graining flow of Γ_k , the scale-dependent effective average action, from the microscopic action $\Gamma_\Lambda = S$ at the UV-cutoff scale Λ to the macroscopic effective average action $\Gamma = \Gamma_0$, which encodes the effective equations of motion for the average fields, all fluctuation effects included. This is facilitated by the regulator R_k which freezes out fluctuations at scales larger than the length scale k^{-1} . The boundary conditions of Γ_k are enforced by requiring $R_\Lambda \sim \infty$ and $R_0 = 0$. Γ_k contains all information about the statistics of the theory with fluctuations until the scale k^{-1} incorporated. For example the inverse of $\Gamma_k^{(2)}$, the second order functional derivative of Γ_k , contains the correlation and response functions.

In general, Eq. (7) can not be solved exactly and one has to resort to an approximation scheme, specified by an ansatz for the scale-dependent effective average action Γ_k and the regulator R_k . Since Eq. (7) does not hinge on the expansion of a small parameter, contrarily to the DRG formalism, these approximations are a priori nonperturbative.

For the regulator, we choose an algebraic cutoff [46], which was previously used in polar active fluids [17], except that it only acts on the wavevector component perpendicular to the collective direction of motion \mathbf{q}_\perp . In Fourier space, it can be written as,

$$R_k(\tilde{\mathbf{q}}, \tilde{\mathbf{p}}) = \mu_{\perp,k} \frac{k^4}{q_\perp^2} \begin{pmatrix} \mathbf{0} & \mathbf{I} & \mathbf{0} & \mathbf{0} \\ \mathbf{I} & \mathbf{0} & \mathbf{0} & \mathbf{0} \\ \mathbf{0} & \mathbf{0} & \mathbf{0} & \mathbf{0} \\ \mathbf{0} & \mathbf{0} & \mathbf{0} & \mathbf{0} \end{pmatrix} \tilde{\delta}_{qp}, \quad (8)$$

where \mathbf{I} denotes a d -dimensional identity matrix, $\tilde{\mathbf{q}} = (\mathbf{q}, \omega_q)$ and $\tilde{\delta}_{qp} = (2\pi)^{d+1} \delta^d(\mathbf{q} + \mathbf{p}) \delta(\omega_q + \omega_p)$. With this regulator choice all momentum integrals appearing in the trace of Eq. (7) can be taken analytically [40].

To confirm whether the results of Ref. [36] remain valid in a nonperturbative setting, we choose an ansatz for Γ_k that contains all terms present in the microscopic action, including the cubic coupling b_k that has been neglected in Ref. [36] and additionally two nonlinear momentum-dependant terms, characterized by $z_k^{(0)}$ and $z_k^{(1)}$,

$$\Gamma_k[\bar{\mathbf{v}}, \mathbf{v}, \bar{\mathcal{P}}, \mathcal{P}] = \int_{\bar{\mathbf{r}}} \left\{ \bar{\mathbf{v}} \cdot \left[\gamma_k \partial_t \mathbf{v} + \lambda_k (\mathbf{v} \cdot \nabla) \mathbf{v} + \nabla \mathcal{P} - \mu_k^\perp \nabla_\perp^2 \mathbf{v} - \mu_k^x \partial_x^2 \mathbf{v} + (a_k + b_k |\mathbf{v}|^2) \mathbf{v} \right] - D_k |\bar{\mathbf{v}}|^2 + \bar{\mathcal{P}} \nabla \cdot \mathbf{v} \right. \\ \left. - z_k^{(0)} \text{Tr} \bar{\mathbf{v}} \nabla_\perp \cdot \left[(|\mathbf{v}|^2 - v_{0,k}^2) \nabla_{\perp,j} \mathbf{v} \right] - z_k^{(1)} \bar{\mathbf{v}} \cdot \partial_x \left[(|\mathbf{v}|^2 - v_{0,k}^2) \partial_x \mathbf{v} \right] \right\}, \quad (9)$$

where $v_{0,k} = \sqrt{|a_k|/b_k}$. Our motivation for including these terms is to (a) check whether b_k is actually an irrelevant coupling as claimed in Ref. [36], (b) try and shift the fixed point location and thus potentially change the value of the scaling exponents, as in the case of the critical $O(N)$ model and many other systems [28, 29], and (c) introduce couplings that could create graphical corrections for the q_x dependent part of the propagator, potentially breaking one of the hyperscaling relations found in the perturbative approach. In the perturbative calculation at one-loop level [36] these graphical correction are vanishing. From a perturbative viewpoint, the additional coupling $z_k^{(1)}$ incorporates higher order loop effects which could change this picture. Note that we could add up to seven additional momentum-dependent nonlinear terms of the same order, but only those included contribute to the self-energy of the Goldstone mode [40]. Further, since the terms containing the pressure field and its response are linear they do not get renormalized [17, 42]. Therefore, we set their coefficients to unity. As derivatives in Eq. (9) are split into contributions parallel and transverse to the x -direction, our ansatz seemingly breaks the rotational symmetry explicitly, however, all couplings can be identified with a fully symmetric ansatz [40]. Finally, nonperturbative contributions could also arise from the regulator choice: due to its dependence on $\mu_{\perp,k}$, the graphical correction of $\mu_{\perp,k}$ will be defined recursively, leading to flow equations that are nonpolynomial in the interaction terms.

The RG flow equations can now be deduced from Eq. (7), evaluated around the expectation value of the velocity $\mathbf{v}(\mathbf{x}, t) = \mathbf{v}_0$ and in the comoving frame by setting external frequencies equal to $\omega = \lambda_k q_x v_0$ [40]. All but the Goldstone mode propagators are set to zero since they are of subleading order [47]. This is also justified a posteriori [40].

Expressing the scale-dependent coefficients in Eq. (9) in dimensionless units (defined in [40] and denoted with

an overbar here), the flow equations read

$$\partial_l \gamma_k = \partial_l D_k = 0, \quad \partial_l \mu_k^\perp = \eta_k^\perp \mu_k^\perp, \quad \partial_l \mu_k^x = \eta_k^x \mu_k^x \quad (10)$$

$$\partial_l \bar{\lambda}_k = \frac{1}{2} \left(4 - d - \frac{5}{2} \eta_k^\perp - \frac{1}{2} \eta_k^x \right) \bar{\lambda}_k, \quad (11)$$

$$\partial_l \bar{b}_k = \left(4 - d - \frac{3}{2} \eta_k^\perp - \frac{1}{2} \eta_k^x \right) \bar{b}_k + f_b, \quad (12)$$

$$\partial_l \bar{z}_k^{(a)} = \left(2 - d - \frac{3 - 2a}{2} \eta_k^\perp - \frac{1 + 2a}{2} \eta_k^x \right) \bar{z}_k^{(a)} + f_z^{(a)}, \quad (13)$$

where $l = -\log k/\Lambda$, and the detailed expressions for the f 's and η 's are given in Ref. [40].

At a fixed point of the flow equations [Eqs. (10)-(13)], the scaling dimension of the Goldstone modes can be extracted from the k -dependence of the equal-time correlation function [contained in $(\Gamma_{k=q}^{(2)})^{-1}$] [40, 48] (in Fourier space),

$$C_T(\mathbf{q}) \equiv \int d\omega \langle \mathbf{u}_T(\mathbf{q}, \omega) \cdot \mathbf{u}_T(-\mathbf{q}, -\omega) \rangle \quad (14) \\ \approx \frac{2D_k}{\gamma_k \mu_k k^2} \int d\bar{\omega} \frac{\delta_{ij} - \hat{x}_i \hat{x}_j - \hat{q}_{\perp,i} \hat{q}_{\perp,j}}{|-i\bar{\omega} + \bar{q}_\perp^2 + \bar{q}_x^2|^2} \Big|_{k=q} \sim q^{\alpha_T},$$

with the dimensionless wavenumbers and frequencies,

$$\bar{q}_\perp = \frac{q_\perp}{k}, \quad \bar{q}_x = \frac{q_x}{k} \sqrt{\frac{\mu_k^x}{\mu_k^\perp}}, \quad \bar{\omega}_\perp = \frac{\omega_\perp \gamma_k}{\mu_k^\perp k^2}, \quad (15)$$

and $\alpha_T = \eta^\perp - 2$. This exponent is related to the other exponents via $2\chi = -\alpha_T - d + 1 - \zeta$.

Note that in our approximation scheme, μ_k^x does acquire a graphical correction (10). If η_k^x were to take a nonzero value at the fixed point, this would imply that the scaling exponents obtained in [36] receive graphical corrections and are thus not exact.

The flow equations [Eqs. (10)-(13)] can be integrated straightforwardly at different initial conditions to obtain the flow diagram, Fig. 1a. Besides the trivial Gaussian FP (yellow pentagon), it contains 3 other nontrivial FPs (modulo the sign of λ_k).

FP 1: On the manifold $\bar{b}_k = 0$, we find the fixed point (blue diamond) whose existence was assumed in Ref. [36]. We have shown here explicitly that it exists (in $d = 3$ the fixed point values are: $\bar{\lambda}_* = \pm 5.5$ and all other couplings vanishing) and confirm the scaling exponents that have previously been found, $\alpha_T = -2(d+1)/5$ (4).

FP 2: On the other manifold, where $\bar{\lambda}_k = 0$, we find the fixed point ($\bar{b}_* = 8.6$ and all other couplings vanishing in $d = 3$) associated to the Goldstone regime of the $O(N)$ model ($N = (d - 1)$ here, since \mathbf{v} is a vector in realspace and one mode is removed by the incompressibility condition). At this fixed point, the scaling behavior of the Goldstone modes remains unmodified from the mean-field behavior $\alpha_T = -2$, however, the mode parallel to the flocking direction, $u_x = \mathbf{u} \cdot \hat{x}$, becomes soft with a scaling dimension $\alpha_x = d - 4$, which is different from mean-field theory, where one would expect this mode to have a finite correlation length [49–52]. In the ERG formalism, this can again be seen from the equal time correlation [analogously defined as in Eq. (14)] [52],

$$C_x(\mathbf{q}) \approx \frac{2D_k}{\gamma_k \mu_k k^2} \int d\bar{\omega} \frac{1}{| -i\bar{\omega} + 2\bar{b}_k \bar{v}_{0,k}^2 + \bar{q}_\perp^2 + \bar{q}_x^2 |^2} \Big|_{k=q}$$

$$\xrightarrow{k \rightarrow 0} \frac{D_k}{2\gamma_k \bar{b}_k v_{0,k}^2} \Big|_{k=q} \sim q^{\alpha_x}, \quad (16)$$

so generally $\alpha_x = \partial_l \log(b_k)$ in the large k limit, since $v_{0,k}$ approaches a fixed value in physical dimensions and D_k and γ_k do not renormalize. Therefore, close to the Gaussian fixed point (yellow pentagon, $l \lesssim 10$ in Fig. 1b and 1c) $\alpha_x = 0$, indicating exponential decay of the correlation function due to a finite correlation length. However, at the Goldstone fixed point (green square), the dimensionless \bar{b}_k takes a fixed point value such that b_k vanishes asymptotically with

$$\alpha_x = d - 4 + \frac{3}{2}\eta^\perp + \frac{1}{2}\eta^x. \quad (17)$$

Since $\eta^\perp = \eta^x = 0$ at this fixed point, we recover $\alpha_x = d - 4$.

The longitudinal mode, parallel to the transverse momentum, $u_L = \hat{\mathbf{q}}_\perp \cdot \mathbf{u}$ is enslaved to the mode in the x -direction via the incompressibility condition $q_\perp u_L = -q_x u_x$, and therefore takes the same scaling dimension $\alpha_L = \alpha_x$, since there is no anisotropic scaling at this fixed point. The RG flow of the couplings and of the scaling dimensions close to this fixed point is shown in Fig. 1b and 1c for values of $15 \lesssim l \lesssim 30$.

FP 3: Now we turn to the attractive fixed point (red circle) that describes generically the ordered phase of IPAF. In this *active Goldstone regime*, both $\bar{\lambda}_k$ and \bar{b}_k take nonvanishing fixed point values and the higher order coupling $z_k^{(0)}$ is generated (in $d = 3$: $\bar{\lambda}_* = \pm 7.1$, $\bar{b}_* = 5.7$, $z_*^{(0)} = -1.4$ and all other couplings vanishing). The coupling $z_k^{(1)}$, however, which generates the anomalous dimension in the x -direction $\eta_k^x \sim z_k^{(1)}$, vanishes such that $\eta_k^x = 0$. Therefore, the scaling behavior of the Goldstone mode remains unmodified compared to the $\bar{b}_k = 0$ fixed point, providing strong evidence that the exponents described in Ref. [36] are indeed exact with $\alpha_T = -2(d + 1)/5$.

Interestingly, as in the equilibrium Goldstone regime, the same argument for the fluctuations in the x -direction (16) applies, yielding again Eq. (17). At this fixed point, however, $\eta^\perp = 2(4 - d)/5$, hence, $\alpha_x = 2(d - 4)/5$. Further, since the scaling at this fixed point is no longer isotropic, we find that the scaling dimension parallel to the transverse momentum differs from that in the x -direction: $\alpha_L = \alpha_x + \eta^x - \eta^\perp = 4(d - 4)/5$. Again, the RG flow of the couplings and of the scaling dimensions close to this fixed point is shown in Fig. 1b and 1c for values of $l \gtrsim 35$.

To recapitulate, in the active Goldstone regime, the fluctuations in the flocking direction (u_x) and longitudinal fluctuations (u_L) become long-ranged due to interactions with the Goldstone modes.

Having determined the values of these additional exponents not considered in Ref. [36], we can further check that they are consistent with the “nonlinear- σ model” picture. Namely, if we assume that

$$\sqrt{|\mathbf{v}_\perp|^2 + v_x^2} = \text{constant}, \quad (18)$$

then $u_x \sim |u_\perp|^2$. Namely, the exponent governing the spatial decay of the equal-time u_x - u_x correlation, χ_x , is exactly 2χ . Hence, $\alpha_x = 2\alpha_T + d - 1 + \zeta$, which gives the expected value of $2(d - 4)/5$. Having found α_x , one can then use the incompressibility condition again to determine the scaling dimension of u_L .

Summary & Outlook.—Our exact renormalization group analysis not only confirms the exact scaling exponents in 3D for incompressible polar active fluids (IPAF) first described in Ref. [36], it also uncovers many novel features of the active matter system. First, we demonstrate the existence of the nontrivial renormalization group (RG) fixed point (as opposed to being presumed in Ref. [36]). Second, we obtain the actual RG flow diagram (Fig. 1a) that i) demonstrates the relevance of the coefficient b_k [associated with the nonlinear term $|\mathbf{v}|^2 \mathbf{v}$ in (1)], which was omitted in the analysis of Ref. [36] [see Eq. (5)], and yet whose presence does not modify the exact scaling exponents; and ii) connects IPAF to the thermal $O(N)$ model (when $\lambda = 0$). Third, we uncover two novel exact scaling exponents that describe the scaling behaviors of \mathbf{u}_L and u_x .

Our work provides convincing evidence that exact scaling exponents (and potentially other universal quantities, such as amplitude ratios) can be obtained using RG methods at non-Gaussian RG fixed points. In particular, exact calculations seem possible for systems where the number of scaling exponents plus allowed graphical corrections is smaller than or equal to the number of relevant coefficients in the equations of motion, as in the case of IPAF considered here. An immediate and important future direction is therefore to identify the precise criteria for exact RG calculations to be possible.

-
- * p.jentsch20@imperial.ac.uk
† c.lee@imperial.ac.uk
- [1] M. Gell-Mann and F. E. Low, Quantum electrodynamics at small distances, *Phys. Rev.* **95**, 1300 (1954).
 - [2] K. Symanzik, Small distance behaviour in field theory and power counting, *Commun.Math. Phys.* **18**, 227 (1970).
 - [3] C. G. Callan, Broken scale invariance in scalar field theory, *Phys. Rev. D* **2**, 1541 (1970).
 - [4] L. P. Kadanoff, Scaling laws for ising models near T_c , *Physics Physique Fizika* **2**, 263 (1966).
 - [5] K. G. Wilson, Renormalization group and critical phenomena. I. Renormalization group and the Kadanoff scaling picture, *Phys. Rev. B* **4**, 3174 (1971).
 - [6] K. G. Wilson, Renormalization group and critical phenomena. II. Phase-space cell analysis of critical behavior, *Phys. Rev. B* **4**, 3184 (1971).
 - [7] P. C. Hohenberg and B. I. Halperin, Theory of dynamic critical phenomena, *Reviews of Modern Physics* **49**, 435 (1977).
 - [8] P. M. Chaikin and T. C. Lubensky, *Principles of Condensed Matter Physics*, 1st ed. (Cambridge University Press, 1995).
 - [9] S. Ramaswamy, The mechanics and statistics of active matter, *Annual Review of Condensed Matter Physics* **1**, 323 (2010).
 - [10] M. C. Marchetti, J. F. Joanny, S. Ramaswamy, T. B. Liverpool, J. Prost, M. Rao, and R. A. Simha, Hydrodynamics of soft active matter, *Reviews of Modern Physics* **85**, 1143 (2013).
 - [11] L. Chen, C. F. Lee, and J. Toner, Moving, reproducing, and dying beyond flatland: Malthusian flocks in dimensions $d > 2$, *Physical Review Letters* **125**, 098003 (2020).
 - [12] S. Mahdisoltani, R. B. A. Zinati, C. Duclut, A. Gambassi, and R. Golestanian, Nonequilibrium polarity-induced chemotaxis: Emergent Galilean symmetry and exact scaling exponents, *Physical Review Research* **3**, 013100 (2021).
 - [13] J. van der Kolk, F. Rasshofer, R. Swiderski, A. Haldar, A. Basu, and E. Frey, Anomalous collective dynamics of auto-chemotactic populations (2022), arXiv:2209.01047 [cond-mat, physics:physics].
 - [14] L. Chen, C. F. Lee, A. Maitra, and J. Toner, Packed swarms on dirt: Two-dimensional incompressible flocks with quenched and annealed disorder, *Physical Review Letters* **129**, 188004 (2022).
 - [15] R. B. A. Zinati, M. Besse, G. Tarjus, and M. Tissier, Dense polar active fluids in a disordered environment, *Phys. Rev. E* **105**, 064605 (2022).
 - [16] A. Cavagna, L. Di Carlo, I. Giardina, T. S. Grigera, S. Melillo, L. Parisi, G. Pisegna, and M. Scandolo, Natural swarms in 3.99 dimensions, *Nature Physics* [10.1038/s41567-023-02028-0](https://doi.org/10.1038/s41567-023-02028-0) (2023).
 - [17] P. Jentsch and C. F. Lee, Critical phenomena in compressible polar active fluids: Dynamical and functional renormalization group studies, *Physical Review Research* **5**, 023061 (2023).
 - [18] P. Jentsch and C. F. Lee, A new universality class describes vicsek's flocking phase in physical dimensions (2024), arXiv:2402.01316 [cond-mat.soft].
 - [19] M. Miller and J. Toner, Phase separation in ordered polar active fluids: A new universality class (2024), arXiv:2401.05996 [cond-mat.soft].
 - [20] K. G. Wilson and M. E. Fisher, Critical exponents in 3.99 dimensions, *Phys. Rev. Lett.* **28**, 240 (1972).
 - [21] K. G. Wilson and J. Kogut, The renormalization group and the ϵ expansion, *Physics Reports* **12**, 75 (1974).
 - [22] C. Wetterich, Exact evolution equation for the effective potential, *Phys. Lett. B* **301**, 90 (1993).
 - [23] U. Ellwanger, Flow equations for N point functions and bound states, *Zeitschrift für Physik C* **62**, 503 (1994).
 - [24] T. R. Morris, The Exact renormalization group and approximate solutions, *Int. J. Mod. Phys. A* **9**, 2411 (1994).
 - [25] N. Dupuis, L. Canet, A. Eichhorn, W. Metzner, J. M. Pawłowski, M. Tissier, and N. Wschebor, The nonperturbative functional renormalization group and its applications, *Physics Reports* **910**, 1 (2021).
 - [26] J. Berges, N. Tetradis, and C. Wetterich, Nonperturbative renormalization flow in quantum field theory and statistical physics, *Physics Reports Renormalization group theory in the new millennium. IV*, **363**, 223 (2002).
 - [27] L. Canet, B. Delamotte, D. Mouhanna, and J. Vidal, Optimization of the derivative expansion in the nonperturbative renormalization group, *Physical Review D* **67**, 065004 (2003).
 - [28] I. Balog, H. Chaté, B. Delamotte, M. Marohnić, and N. Wschebor, Convergence of nonperturbative approximations to the renormalization group, *Phys. Rev. Lett.* **123**, 240604 (2019).
 - [29] G. De Polsi, I. Balog, M. Tissier, and N. Wschebor, Precision calculation of critical exponents in the O(N) universality classes with the nonperturbative renormalization group, *Phys. Rev. E* **101**, 042113 (2020).
 - [30] J.-P. Blaizot, R. Méndez-Galain, and N. Wschebor, A new method to solve the non-perturbative renormalization group equations, *Physics Letters B* **632**, 571 (2006).
 - [31] F. Benitez, J.-P. Blaizot, H. Chaté, B. Delamotte, R. Méndez-Galain, and N. Wschebor, Solutions of renormalization-group flow equations with full momentum dependence, *Physical Review E* **80**, 030103 (2009).
 - [32] F. Benitez, J.-P. Blaizot, H. Chaté, B. Delamotte, R. Méndez-Galain, and N. Wschebor, Nonperturbative renormalization group preserving full-momentum dependence: Implementation and quantitative evaluation, *Physical Review E* **85**, 026707 (2012).
 - [33] D. Forster, D. R. Nelson, and M. J. Stephen, Large-distance and long-time properties of a randomly stirred fluid, *Physical Review A* **16**, 732 (1977).
 - [34] T. Hwa and M. Kardar, Dissipative transport in open systems: An investigation of self-organized criticality, *Physical Review Letters* **62**, 1813 (1989).
 - [35] J. Toner and Y. Tu, Long-range order in a two-dimensional dynamical XY model: How birds fly together, *Physical Review Letters* **75**, 4326 (1995).
 - [36] L. Chen, C. F. Lee, and J. Toner, Incompressible polar active fluids in the moving phase in dimensions $d > 2$, *New Journal of Physics* **20**, 113035 (2018).
 - [37] J. Toner, N. Guttenberg, and Y. Tu, Swarming in the Dirt: Ordered Flocks with Quenched Disorder, *Physical Review Letters* **121**, 248002 (2018).
 - [38] L. Chen, C. F. Lee, A. Maitra, and J. Toner, Incompressible polar active fluids with quenched random field disorder in dimensions $d > 2$, *Physical Review Letters* **129**, 198001 (2022).

- [39] L. Canet, H. Chaté, and B. Delamotte, General framework of the non-perturbative renormalization group for non-equilibrium steady states, *Journal of Physics A* **44**, 495001 (2011).
- [40] Supplemental material.
- [41] P. Tomassini, An exact renormalization group analysis of 3D well developed turbulence, *Physics Letters B* **411**, 117 (1997).
- [42] L. Canet, B. Delamotte, and N. Wschebor, Fully developed isotropic turbulence: Symmetries and exact identities, *Physical Review E* **91**, 053004 (2015).
- [43] P. C. Martin, E. D. Siggia, and H. A. Rose, Statistical dynamics of classical systems, *Physical Review A* **8**, 423 (1973).
- [44] C. de Dominicis, Techniques de renormalisation de la théorie des champs et dynamique des phénomènes critiques, *Le Journal de Physique Colloques* **37**, C1 (1976).
- [45] H. K. Janssen, On a Lagrangean for classical field dynamics and renormalization group calculations of dynamical critical properties, *Zeitschrift für Physik B Condensed Matter and Quanta* **23**, 377 (1976).
- [46] T. R. Morris, Derivative expansion of the exact renormalization group, *Physics Letters B* **329**, 241 (1994).
- [47] Technically, there one contributing term, which we have included. See, [40].
- [48] J.-P. Blaizot, R. Méndez-Galain, and N. Wschebor, Non-perturbative renormalization group and momentum dependence of n -point functions. I, *Physical Review E* **74**, 051116 (2006).
- [49] A. Z. Patashinskii and V. L. Pokrovskii, Longitudinal susceptibility and correlations in degenerate systems, *Zh. Eksp. Teor. Fiz.* **64**, 1445 (1973).
- [50] M. E. Fisher, M. N. Barber, and D. Jasnow, Helicity modulus, superfluidity, and scaling in isotropic systems, *Physical Review A* **8**, 1111 (1973).
- [51] R. Anishetty, R. Basu, N. D. H. Dass, and H. S. Sharatchandra, Infrared behavior of systems with goldstone bosons, *International Journal of Modern Physics A* **14**, 3467 (1999).
- [52] N. Dupuis, Infrared behavior in systems with a broken continuous symmetry: Classical $O(N)$ model versus interacting bosons, *Physical Review E* **83**, 31120 (2011).

Supplemental material for Can exact scaling exponents be obtained using RG? An illustration in incompressible polar active fluids

Patrick Jentsch* and Chiu Fan Lee†
Department of Bioengineering, Imperial College London,
South Kensington Campus, London SW7 2AZ, U.K.

(Dated: April 19, 2024)

ANSATZ AND LINEAR ANALYSIS

The ansatz for the effective action Γ_k presented in the main text looks like it breaks the continuous rotational symmetry of the theory explicitly, since it contains couplings for terms with derivatives oriented in the flocking direction and perpendicular to it. It is however equivalent to the following ansatz that manifestly respects the rotational symmetries,

$$\Gamma_k[\bar{\mathbf{v}}, \mathbf{v}, \bar{\mathcal{P}}, \mathcal{P}] = \int_{\tilde{\mathbf{r}}} \left[\bar{\mathcal{P}} \nabla_i v_i - D_k \bar{v}_i \bar{v}_i + \bar{v}_i \cdot \left\{ \gamma_k \partial_t v_i + \lambda_k (v_j \cdot \nabla_j) v_i + \nabla_i \mathcal{P} + U'_k(\kappa) v_i \right. \right. \\ \left. \left. - \nabla_j (Z_k(\kappa) \nabla_j v_i) - \nabla_j (Y_k(\kappa) v_j v_m \nabla_m v_i) \right\} \right], \quad (1)$$

where $\kappa = |\mathbf{v}|^2/2$ and the term U'_k is defined as a derivative such that U_k is the scale-dependent effective potential. The two-point functions associated to this ansatz, evaluated in a uniform background field ($\bar{\mathbf{v}} = \bar{\mathcal{P}} = \mathcal{P} = 0$, $\mathbf{v} = \mathbf{v}_u$) are,

$$\Gamma_{k,ij}^{(2,0,0,0)}[0, \mathbf{v}_u, 0, 0](\tilde{\mathbf{q}}, \tilde{\mathbf{p}}) = -2D_k \delta_{ij} \tilde{\delta}_{qp}, \quad (2)$$

$$\Gamma_{k,ij}^{(1,1,0,0)}[0, \mathbf{v}_u, 0, 0](\tilde{\mathbf{q}}, \tilde{\mathbf{p}}) = \left\{ [-i\gamma_k \omega_q + i\lambda_k v_u q_x + U'_k(\kappa_u) + Z_k(\kappa_u) q^2 + Y_k(\kappa_u) (\mathbf{v}_u \cdot \mathbf{q})^2] \delta_{ij} + U''_k(\kappa_u) v_{u,i} v_{u,j} \right\} \tilde{\delta}_{qp}, \quad (3)$$

$$\Gamma_{k,i}^{(1,0,0,1)}[0, \mathbf{v}_u, 0, 0](\tilde{\mathbf{q}}, \tilde{\mathbf{p}}) = i q_i, \quad (4)$$

$$\Gamma_{k,i}^{(0,1,1,0)}[0, \mathbf{v}_u, 0, 0](\tilde{\mathbf{q}}, \tilde{\mathbf{p}}) = -i q_i, \quad (5)$$

where we have used the following identities,

$$\frac{\delta}{\delta v_j(\tilde{\mathbf{q}})} v_i(\tilde{\mathbf{r}}) = \delta_{ij} e^{i\omega_q t - i\mathbf{q} \cdot \mathbf{r}}, \quad \frac{\delta}{\delta \bar{v}_j(\tilde{\mathbf{q}})} \bar{v}_i(\tilde{\mathbf{r}}) = \delta_{ij} e^{i\omega_q t - i\mathbf{q} \cdot \mathbf{r}}, \quad \frac{\delta}{\delta \mathcal{P}(\tilde{\mathbf{q}})} \mathcal{P}(\tilde{\mathbf{r}}) = e^{i\omega_q t - i\mathbf{q} \cdot \mathbf{r}}, \quad \frac{\delta}{\delta \bar{\mathcal{P}}(\tilde{\mathbf{q}})} \bar{\mathcal{P}}(\tilde{\mathbf{r}}) = e^{i\omega_q t - i\mathbf{q} \cdot \mathbf{r}}, \quad (6)$$

which also define our Fourier-Conventions. Note that the only difference between the contribution in the x -direction and the isotropic term is generated by U_k , which will lead to the freezing out of the correlations in this direction. In general, we could write down 7 other terms at the same order in derivatives as the terms characterized by Z_k and Y_k , however, since those would not be isotropic, their linear contributions would only contribute to the subleading x - or longitudinal modes or create nonlinear couplings to the same modes. Both effects would be vanishing in the small k limit anyways.

By expanding the functions around the minimum of the potential, $\mathbf{v}_{0,k}$, where $U'_k(\kappa_{0,k}) = 0$ we can identify the couplings from the main-text as,

$$a_k = 2\kappa_{0,k} U''_k(\kappa_{0,k}), \quad b_k = U''_k(\kappa_{0,k}), \quad \mu_k^\perp = Z_k(\kappa_{0,k}), \quad \mu_k^x = Z_k(\kappa_{0,k}) + 2Y_k(\kappa_{0,k}) \kappa_{0,k}, \quad (7)$$

$$z_k^{(0)} = Z'_k(\kappa_{0,k}), \quad z_k^{(1)} = Z'_k(\kappa_{0,k}) + 2Y_k(\kappa_{0,k}). \quad (8)$$

All couplings can therefore be obtained from the two-point function, such that all flow equations can be obtained from the second-order functional derivative of the Wetterich equation,

$$\partial_l \Gamma_k^{(2)} = \partial_l \left[-\frac{1}{2} \text{Tr} \Gamma_k^{(4)} \mathcal{G}_k + \text{Tr} \Gamma_k^{(3)} \mathcal{G}_k \Gamma_k^{(3)} \mathcal{G}_k \right]_{k'=k}, \quad (9)$$

with \mathcal{G}_k being the regulated propagator

$$\mathcal{G}_k = \left(\Gamma_k^{(2)} + R_{k'} \right)^{-1}, \quad (10)$$

and k and k' are being treated as independent scale variables, such that $\partial_{l'}$ only acts on the k -dependence of the regulator. Defining,

$$G_{k,ij}^{-1}(\tilde{\mathbf{q}}) = \frac{1}{VT} \Gamma_{k,ij}^{(1,1,0,0)}[0, \mathbf{v}_u, 0, 0](\tilde{\mathbf{q}}, -\tilde{\mathbf{q}}), \quad (11)$$

where $VT = (2\pi)^{d+1} \delta^{d+1}(0)$ is the spatiotemporal Volume, the unregulated propagator $\tilde{\mathcal{G}}_k$ can be obtained by inverting the two-point function $\Gamma^{(2)}$,

$$\tilde{\mathcal{G}}_k = \left(\Gamma^{(2)} \right)^{-1} = \begin{pmatrix} -2D_k & \mathbf{G}_k^{-1}(\tilde{\mathbf{q}}) & 0 & \mathbf{i}\mathbf{q} \\ (\mathbf{G}_k^T)^{-1}(-\tilde{\mathbf{q}}) & 0 & -\mathbf{i}\mathbf{q} & 0 \\ 0 & \mathbf{i}\mathbf{q}^T & 0 & 0 \\ -\mathbf{i}\mathbf{q}^T & 0 & 0 & 0 \end{pmatrix}^{-1} \quad (12)$$

$$= \begin{pmatrix} 0 & \mathbf{G}_{k,\perp}^T(-\tilde{\mathbf{q}}) & 0 & \mathbf{P}_l^T(-\tilde{\mathbf{q}}) \\ \mathbf{G}_{k,\perp}(\tilde{\mathbf{q}}) & 2D_k \mathbf{G}_{k,\perp}(\tilde{\mathbf{q}}) \cdot \mathbf{G}_{k,\perp}^T(-\tilde{\mathbf{q}}) & \mathbf{P}_r(\tilde{\mathbf{q}}) & 2D_k \mathbf{G}_{k,\perp}(\tilde{\mathbf{q}}) \cdot \mathbf{P}_l^T(-\tilde{\mathbf{q}}) \\ 0 & \mathbf{P}_r^T(-\tilde{\mathbf{q}}) & 0 & \frac{-\mathbf{i}\mathbf{P}_r^T(-\tilde{\mathbf{q}}) \cdot (\mathbf{G}_k^T)^{-1}(-\tilde{\mathbf{q}}) \cdot \mathbf{q}}{q^2} \\ \mathbf{P}_l(\tilde{\mathbf{q}}) & 2D_k \mathbf{P}_l(\tilde{\mathbf{q}}) \cdot \mathbf{G}_{k,\perp}^T(-\tilde{\mathbf{q}}) & \frac{\mathbf{i}\mathbf{q}^T \cdot \mathbf{G}_k^{-1}(\tilde{\mathbf{q}}) \cdot \mathbf{P}_r(\tilde{\mathbf{q}})}{q^2} & 2D_k \mathbf{P}_l(\tilde{\mathbf{q}}) \cdot \mathbf{P}_l^T(-\tilde{\mathbf{q}}) \end{pmatrix} \quad (13)$$

where we have defined,

$$\mathbf{P}_r(\tilde{\mathbf{q}}) = \frac{-\mathbf{i}\mathbf{q} + \mathbf{i}\mathbf{G}_{k,\perp}(\tilde{\mathbf{q}}) \cdot \mathbf{G}_k^{-1}(\tilde{\mathbf{q}}) \cdot \mathbf{q}}{q^2}, \quad \mathbf{P}_l(\tilde{\mathbf{q}}) = \frac{-\mathbf{i}\mathbf{q}^T + \mathbf{i}\mathbf{q}^T \cdot \mathbf{G}_k^{-1}(\tilde{\mathbf{q}}) \cdot \mathbf{G}_{k,\perp}(\tilde{\mathbf{q}})}{q^2}, \quad (14)$$

and the transverse propagator,

$$\mathbf{G}_{k,\perp} = \mathbf{G}_{k,x_\perp} + \mathbf{G}_{k,T}, \quad (15)$$

with,

$$\mathbf{G}_{k,x_\perp}(\tilde{\mathbf{q}}) = G_{k,x_\perp}(\tilde{\mathbf{q}}) \mathbf{P}_{x_\perp}(\mathbf{q}) = \frac{\mathbf{P}_{x_\perp}(\mathbf{q})}{-\mathbf{i}\gamma_k \omega_q + a_k \frac{q_\perp^2}{q^2} + \mathbf{i}\lambda_k v_0 q_x + \mu_k^\perp q_\perp^2 + \mu_k^x q_x^2} \quad (16)$$

$$\mathbf{G}_{k,T}(\tilde{\mathbf{q}}) = G_{k,T}(\tilde{\mathbf{q}}) \mathbf{P}_T(\mathbf{q}) = \frac{\mathbf{P}_T(\mathbf{q})}{-\mathbf{i}\gamma_k \omega_q + \mathbf{i}\lambda_k v_0 q_x + \mu_k^\perp q_\perp^2 + \mu_k^x q_x^2}, \quad (17)$$

and

$$P_{x_\perp,ij}(\mathbf{q}) = \left(\frac{q_\perp}{q} \hat{x}_i - \frac{q_x}{q} \hat{q}_{\perp,i} \right) \left(\frac{q_\perp}{q} \hat{x}_j - \frac{q_x}{q} \hat{q}_{\perp,j} \right) \quad (18)$$

$$P_{T,ij}(\mathbf{q}) = \delta_{ij} - \hat{x}_i \hat{x}_j - \hat{q}_{\perp,i} \hat{q}_{\perp,j}, \quad (19)$$

which are the projector parallel to the component of $\hat{\mathbf{x}}$ that is perpendicular to \mathbf{q} and the projector transverse to both \mathbf{q} and $\hat{\mathbf{x}}$ respectively. The contributions from the pressure term, produce precisely the desired effect that all velocity correlation and response functions (corresponding to $\bar{\mathbf{v}}$ and \mathbf{v} entries) are transverse to the wavevector \mathbf{q} . Most of the correlation functions involving the pressure \mathcal{P} or its response field $\bar{\mathcal{P}}$ (corresponding to all other entries) are nonzero, but do not enter the RG calculation since there are no interaction terms involving the pressure. To represent the graphical corrections diagrammatically later, we also adopt a graphical notation for these two propagators,

$$i \xrightarrow{\tilde{\mathbf{q}}} j = \mathbf{G}_{k,T,ij}(\tilde{\mathbf{q}}), \quad (20)$$

$$i \cdots \xrightarrow{\tilde{\mathbf{q}}} \cdots j = \mathbf{G}_{k,x_\perp,ij}(\tilde{\mathbf{q}}), \quad (21)$$

and the noise term,

$$i \rightarrow \otimes \leftarrow j = 2D_k . \quad (22)$$

External lines never imply a propagator (except in Eqns. (20), (21) and (43)).

Further, from the two-point function $\tilde{\mathcal{G}}_k$, the correlation function \mathbf{C}_\perp can be obtained, given by the (\mathbf{v}, \mathbf{v}) entry of $\tilde{\mathcal{G}}_k$, i.e.,

$$\mathbf{C}_\perp(\tilde{\mathbf{q}}) = 2D_k \mathbf{G}_{k,\perp}(\tilde{\mathbf{q}}) \cdot \mathbf{G}_{k,\perp}^T(-\tilde{\mathbf{q}}) . \quad (23)$$

Note, that $q_x^2 \mathbf{C}_{xx} = q_\perp^2 \mathbf{C}_{q_\perp q_\perp}$, as expected from the incompressibility condition $q_x u_x + q_\perp u_\perp = 0$.

Since the contribution of \mathbf{G}_{k,x_\perp} is massive, i.e., a_k has a linear scaling dimension of 2, it will freeze out during the RG-flow and no longer contribute in the large-scale limit. We can therefore make the approximation that

$$\mathbf{G}_{k,x_\perp} = \mathbf{P}_{x_\perp}(\mathbf{q}) \frac{q^2}{a_k q_\perp^2} , \quad (24)$$

which will become exact in the limit $k \rightarrow 0$. In most diagrams one can even set $\mathbf{G}_{k,x_\perp} = 0$ directly, leading to the vanishing of that diagram. However, there is one diagram that needs to be treated more carefully, which is discussed below.

By shifting the frequency $\omega_q \rightarrow \omega_q + q_x \lambda_k v_{0,k} / \gamma_k$, the only other coupling with positive scaling dimension, i.e., $\lambda_k v_0$, can be removed from the propagator. It corresponds to a Galilei shift to the comoving frame. As we show later, this can be done for both internal as well as external frequencies for all graphical corrections appearing later.

REGULATOR CHOICE

As the regulator, we choose an algebraic cutoff,

$$R_k(\tilde{\mathbf{q}}, \tilde{\mathbf{p}}) = \mu_{\perp,k} \frac{k^4}{q_\perp^2} \begin{pmatrix} \mathbf{0} & \mathbf{I} & \mathbf{0} & \mathbf{0} \\ \mathbf{I} & \mathbf{0} & \mathbf{0} & \mathbf{0} \\ \mathbf{0} & \mathbf{0} & \mathbf{0} & \mathbf{0} \\ \mathbf{0} & \mathbf{0} & \mathbf{0} & \mathbf{0} \end{pmatrix} \tilde{\delta}_{qp} , \quad (25)$$

where,

$$r(y) = \frac{1}{y} \quad (26)$$

and that acts only on transverse momenta. With this choice, all integrals appearing in the graphical corrections can be taken analytically and, since the regulator is frequency independent, causality is preserved naturally. Since the regulator modifies the linear theory only by an isotropic term, the regulated propagators are obtained straightforwardly,

$$G_{k,x_\perp}(\tilde{\mathbf{q}}) = \frac{1}{-i\gamma_k \omega_q + a_k \frac{q_\perp^2}{q^2} + i\lambda_k v_0 q_x + \mu_k^\perp q_\perp^2 + \mu_k^x q_x^2 + \mu_k^\perp k'^2 r(q_\perp^2/k'^2)} \quad (27)$$

$$G_{k,T}(\tilde{\mathbf{q}}) = \frac{1}{-i\gamma_k \omega_q + i\lambda_k v_0 q_x + \mu_k^\perp q_\perp^2 + \mu_k^x q_x^2 + \mu_k^\perp k'^2 r(q_\perp^2/k'^2)} . \quad (28)$$

The limit from Eq. (24), which must be taken in dimensionless units, is still valid in the regulated theory. Further, since the scale derivative of (25),

$$\partial_t R_k(\tilde{\mathbf{q}}, \tilde{\mathbf{p}}) = (\eta_k^\perp - 4) \mu_{\perp,k} \frac{k^4}{q_\perp^2} \begin{pmatrix} \mathbf{0} & \mathbf{I} & \mathbf{0} & \mathbf{0} \\ \mathbf{I} & \mathbf{0} & \mathbf{0} & \mathbf{0} \\ \mathbf{0} & \mathbf{0} & \mathbf{0} & \mathbf{0} \\ \mathbf{0} & \mathbf{0} & \mathbf{0} & \mathbf{0} \end{pmatrix} \tilde{\delta}_{qp} , \quad (29)$$

depends on η_k^\perp , the flow equation for μ_k^\perp defines a recursion relation for η_k^\perp , the solution of which is nonpolynomial in at least some of the couplings. For instance, the nonperturbative nature of using such a regulator is enough to reveal

the nonperturbative fixed point of the KPZ equation in the RG flow [1], even if the scaling exponents are not well described in this case. We therefore use this regulator to check whether the same effect plays a role for incompressible polar active fluids.

We have also studied the following regulator with a sharp cutoff,

$$R_k(\tilde{\mathbf{q}}, \tilde{\mathbf{p}}) = -2D [\Theta(|\mathbf{q}_\perp| - k) - 1] \begin{pmatrix} \mathbf{I} & \mathbf{0} & \mathbf{0} & \mathbf{0} \\ \mathbf{0} & \mathbf{0} & \mathbf{0} & \mathbf{0} \\ \mathbf{0} & \mathbf{0} & 0 & 0 \\ \mathbf{0} & \mathbf{0} & 0 & 0 \end{pmatrix} \tilde{\delta}_{qp}, \quad (30)$$

which also allows for an analytic solution of the same integrals as with the algebraic regulator, however, we found that the resulting RG-flow becomes divergent in $d = 3$. In larger dimensions, the scaling exponents presented in the main paper remained however unchanged. Since it has been shown previously, that sharp regulators can produce unreliable results in nontrivial FRG approximations [2], we believe that the observed divergence at $d = 3$ was an artifact of using this particular regulator.

RG FLOW EQUATIONS

As outlined above, the flow equations for all couplings (7)-(8) can be obtained from Eq. (9), for which we still need to determine the vertices $\Gamma_k^{(3)}$ and $\Gamma_k^{(4)}$. The only nonvanishing components of these vertices are

$$\begin{aligned} \Gamma_{ijk}^{(1,2,0,0)}(\tilde{\mathbf{q}}, \tilde{\mathbf{h}}, \tilde{\mathbf{k}}) &= [-i\lambda_k(k_j\delta_{ik} + h_k\delta_{ij}) + b_kv_{0,k}(\delta_{ij}\hat{x}_k + \delta_{jk}\hat{x}_i + \delta_{ki}\hat{x}_j) \\ &\quad - z_k^{(0)}v_{0,k}(\delta_{ij}\hat{x}_k\mathbf{q}_\perp \cdot \mathbf{h}_\perp + \delta_{ik}\hat{x}_j\mathbf{q}_\perp \cdot \mathbf{k}_\perp) \\ &\quad - z_k^{(1)}v_{0,k}(\delta_{ij}\hat{x}_kq_xh_x + \delta_{ik}\hat{x}_jq_xk_x)] \tilde{\delta}_{qhk}, \end{aligned} \quad (31)$$

$$\begin{aligned} \Gamma_{ijkl}^{(1,3,0,0)}(\tilde{\mathbf{q}}, \tilde{\mathbf{h}}, \tilde{\mathbf{k}}, \tilde{\mathbf{l}}) &= [b_k(\delta_{kl}\delta_{ij} + \delta_{jl}\delta_{ik} + \delta_{il}\delta_{kj}) \\ &\quad - z_k^{(0)}(\delta_{ij}\delta_{kl}\mathbf{q}_\perp \cdot \mathbf{h}_\perp + \delta_{ik}\delta_{jl}\mathbf{q}_\perp \cdot \mathbf{k}_\perp + \delta_{il}\delta_{jk}\mathbf{q}_\perp \cdot \mathbf{l}_\perp) \\ &\quad - z_k^{(1)}(\delta_{ij}\delta_{kl}q_xh_x + \delta_{ik}\delta_{jl}q_xk_x + \delta_{il}\delta_{jk}q_xl_x)] \tilde{\delta}_{qhk}. \end{aligned} \quad (32)$$

Imposing momentum conservation at each vertex, we introduce their graphical notation,

$$\begin{array}{c} \mathbf{h}, j \\ \nearrow \quad \searrow \\ \mathbf{q}, i \quad \mathbf{q} - \mathbf{h}, k \end{array} = \frac{1}{VT} \Gamma_{ijk}^{(1,2,0,0)}(\tilde{\mathbf{q}}, -\tilde{\mathbf{h}}, \tilde{\mathbf{h}} - \tilde{\mathbf{q}}), \quad (33)$$

$$\begin{array}{c} \mathbf{h}, j \\ \nearrow \quad \searrow \\ \mathbf{q}, i \quad \mathbf{k}, k \\ \nwarrow \quad \nearrow \\ \mathbf{q} - \mathbf{h} - \mathbf{k}, l \end{array} = \frac{1}{VT} \Gamma_{ijkl}^{(1,3,0,0)}(\tilde{\mathbf{q}}, -\tilde{\mathbf{h}}, -\tilde{\mathbf{k}}, \tilde{\mathbf{h}} + \tilde{\mathbf{k}} - \tilde{\mathbf{q}}) \quad (34)$$

where both propagators [Eqns. (27) and (28)] can connect to any of the in- or outgoing lines.

The graphical corrections to the 2-point functions,

$$\mathbf{F}_v(q_x, \mathbf{q}_\perp, \omega_q) = \frac{1}{VT} \left. \partial_l \Gamma_k^{(\bar{\mathbf{v}}\mathbf{v})} \right|_{\bar{\mathbf{v}}=0, \mathbf{v}=\hat{\mathbf{x}}v_{0,k}, \bar{\mathcal{P}}=0, \mathcal{P}=0} = \frac{1}{VT} \left. \frac{\delta^2 \partial_l \Gamma_k}{\delta \bar{\mathbf{v}}(\tilde{\mathbf{q}}) \delta \mathbf{v}(-\tilde{\mathbf{q}})} \right|_{\bar{\mathbf{v}}=0, \mathbf{v}=\hat{\mathbf{x}}v_{0,k}, \bar{\mathcal{P}}=0, \mathcal{P}=0}, \quad (35)$$

$$\mathbf{F}_D(q_x, \mathbf{q}_\perp, \omega_q) = \frac{1}{VT} \left. \partial_l \Gamma_k^{(\bar{\mathbf{v}}\bar{\mathbf{v}})} \right|_{\bar{\mathbf{v}}=0, \mathbf{v}=\hat{\mathbf{x}}v_{0,k}, \bar{\mathcal{P}}=0, \mathcal{P}=0} = \frac{1}{VT} \left. \frac{\delta^2 \partial_l \Gamma_k}{\delta \bar{\mathbf{v}}(\tilde{\mathbf{q}}) \delta \bar{\mathbf{v}}(-\tilde{\mathbf{q}})} \right|_{\bar{\mathbf{v}}=0, \mathbf{v}=\hat{\mathbf{x}}v_{0,k}, \bar{\mathcal{P}}=0, \mathcal{P}=0}, \quad (36)$$

can then be represented as,

$$\mathbf{F}_g(\tilde{\mathbf{q}}) = \frac{1}{2} \left(\text{Diagram 1} - \text{Diagram 2} - \text{Diagram 3} \right), \quad (37)$$

$$\mathbf{F}_D(0) = 0. \quad (38)$$

Here, we have already set to zero all diagrams that contain the \mathbf{G}_{k,x_\perp} -propagator, except for the last diagram in Eq. (37) hinted at above. The reason is that the three-point vertices contain contributions proportional to $v_{0,k}$, which diverges in dimensionless units, such that the total diagram remains finite. Since the first diagram in Eq. (37) is independent of frequencies, the tilde on the wavevectors has been omitted. The usual Feynman rules apply and the ∂'_l derivative needs to still be applied to each expression. Internal wavenumbers and frequencies are not written explicitly.

Plugging in the expressions for each diagram, we find,

$$\begin{aligned} \text{Diagram 1} &= 2D_k \partial_{l'} \int_{\tilde{\mathbf{h}}} \left[G_{k,T}(\tilde{\mathbf{h}}) G_{k,T}(-\tilde{\mathbf{h}}) \right] \\ &\times \left\{ b_k [(d-2)\delta_{ij} + 2P_{T,ij}(\mathbf{h})] + (d-2)\delta_{ij} \left(z_k^{(0)} q_\perp^2 + z_k^{(1)} q_x^2 \right) \right\} \Big|_{k'=k}, \end{aligned} \quad (39)$$

$$\begin{aligned} \text{Diagram 2} &= 2D_k \partial_{l'} \int_{\tilde{\mathbf{h}}} \left[P_{T,mn}(\mathbf{h}) G_{k,T}(\tilde{\mathbf{h}}) G_{k,T}(-\tilde{\mathbf{h}}) P_{T,kl}(\mathbf{q} - \mathbf{h}) G_{k,T}(\tilde{\mathbf{q}} - \tilde{\mathbf{h}}) \right] \\ &\times [\text{i}\lambda_k(q_m \delta_{ik} + h_k \delta_{im}) + b_k v_{0,k} \delta_{mk} \hat{x}_i] \\ &\times \left[\text{i}\lambda_k(q_n \delta_{lj} - h_j \delta_{ln}) + b_k v_{0,k} \delta_{ln} \hat{x}_j + z_k^{(0)} v_{0,k} (\delta_{ln} \hat{x}_j [\mathbf{h}_\perp - \mathbf{q}_\perp] \cdot \mathbf{h}_\perp) + z_k^{(1)} v_{0,k} (\delta_{ln} \hat{x}_j [h_x - q_x] h_x) \right] \Big|_{k'=k}, \end{aligned} \quad (40)$$

$$\begin{aligned} \text{Diagram 3} &= 2D_k \partial_{l'} \int_{\tilde{\mathbf{h}}} \left[P_{T,mn}(\mathbf{h}) G_{k,T}(\tilde{\mathbf{h}}) G_{k,T}(-\tilde{\mathbf{h}}) P_{x_\perp,kl}(\mathbf{q} - \mathbf{h}) G_{k,x_\perp}(\tilde{\mathbf{q}} - \tilde{\mathbf{h}}) \right] \\ &\times \left[\text{i}\lambda_k(q_m \delta_{ik} + h_k \delta_{im}) + b_k v_{0,k} (\delta_{im} \hat{x}_k + \delta_{mk} \hat{x}_i) + z_k^{(0)} v_0 \delta_{im} \hat{x}_k \mathbf{q}_\perp \cdot \mathbf{h}_\perp + z_k^{(1)} v_0 \delta_{im} \hat{x}_k q_x h_x \right] \\ &\times \left[\text{i}\lambda_k(q_n \delta_{lj} - h_j \delta_{ln}) + b_k v_{0,k} (\delta_{ln} \hat{x}_j + \delta_{nj} \hat{x}_l) + z_k^{(0)} v_{0,k} \delta_{ln} \hat{x}_j [\mathbf{h}_\perp - \mathbf{q}_\perp] \cdot \mathbf{h}_\perp + z_k^{(1)} v_{0,k} \delta_{ln} \hat{x}_j [h_x - q_x] h_x \right] \Big|_{k'=k}. \end{aligned} \quad (41)$$

Projecting Eq. (41) transverse to both $\hat{\mathbf{x}}$ and \mathbf{q} , plugging in Eq. (24), using $a_k = 2\kappa_{0,k} b_k = v_{0,k}^2 b_k$ and taking the limit $v_{0,k} \rightarrow \infty$ (technically speaking, in these physical dimensions, $v_{0,k}$ remains finite and all other couplings become small, but the effect is the same), it simplifies to,

$$P_{T,im}(\mathbf{q}) \text{Diagram 4} P_{T,nj} = 2D_k \partial_{l'} \int_{\tilde{\mathbf{h}}} \left[G_{k,T}(\tilde{\mathbf{h}}) G_{k,T}(-\tilde{\mathbf{h}}) \right] \left\{ b_k P_{T,im}(\mathbf{q}) P_{T,mn}(\mathbf{h}) P_{T,nj}(\mathbf{q}) \right\} \Big|_{k'=k}, \quad (42)$$

where some terms vanished due to antisymmetry with respect to reflection of the \mathbf{h} integration. From the form in Eq. (42) one can see that it cancels out the term proportional to $P_{T,ij}(\mathbf{h})$ from Eq. (39), once it is projected transverse to both $\hat{\mathbf{x}}$ and \mathbf{q} and equipped with the prefactors from Eq. (37). This effect is related to the fact that if one were to solve the EOM for u_x in the large scale-limit, it would remove the nonlinearity arising from the b_k coupling (i.e. in the equilibrium limit, where $\lambda_k = 0$, the Goldstone modes becomes effectively Gaussian). The fact that b_k is still a coupling that plays a role in this RG-calculation is that this cancellation will only happen fully on the tree level. Our approach however is based on the effective action, i.e., the 1PI-generating functional, where tree-level effects are intentionally removed. In other words, the 1-PI 4-vertex is finite but will be cancelled out by tree diagrams when calculating, e.g., the 4-point correlation functions after the effective action has been determined, i.e., when $k = 0$.

For example, in the following correlation function,

$$\begin{aligned} &\left\langle v_{T,i}(\tilde{\mathbf{q}}) \bar{v}_{T,j}(\tilde{\mathbf{j}}) \bar{v}_{T,k}(\tilde{\mathbf{k}}) \bar{v}_{T,l}(\tilde{\mathbf{l}}) \right\rangle \\ &= - \text{Diagram 5} + \text{Diagram 6} + \text{Diagram 7} + \text{Diagram 8} \\ &= 0, \end{aligned} \quad (43)$$

only the first diagram is a 1-PI contribution, which is nonzero. However, the three following diagrams cancel its contribution in the limit of small k , such that the correlation function vanishes. In Eq (43), external lines do correspond to a propagator.

From the \mathbf{F} 's the flow equations for all the couplings [Eqns. (7)-(8)] can be projected:

$$\partial_l \kappa_{0,k} = -\frac{1}{b_k} \frac{1}{d-2} [\text{Tr} \mathbf{P}_T(\mathbf{q}) \mathbf{F}_v(q_x, \mathbf{q}_\perp, \omega_q + q_x \lambda_k / \gamma_k v_{0,k})]_{\bar{\mathbf{q}}=0}, \quad (44)$$

$$\partial_l \gamma_k = \frac{i}{d-2} \left[\frac{\partial}{\partial \omega_q} \text{Tr} \mathbf{P}_T(\mathbf{q}) \mathbf{F}_g(q_x, \mathbf{q}_\perp, \omega_q + q_x \lambda_k / \gamma_k v_{0,k}) \right]_{\bar{\mathbf{q}}=0}, \quad (45)$$

$$\partial_l \mu_k^\perp = \frac{1}{2(d-2)} \left[\frac{\partial^2}{\partial q_\perp^2} \text{Tr} \mathbf{P}_T(\mathbf{q}) \mathbf{F}_g(q_x, \mathbf{q}_\perp, \omega_q + q_x \lambda_k / \gamma_k v_{0,k}) \right]_{\bar{\mathbf{q}}=0}, \quad (46)$$

$$\partial_l \mu_k^x = \frac{1}{2(d-2)} \left[\frac{\partial^2}{\partial q_x^2} \text{Tr} \mathbf{P}_T(\mathbf{q}) \mathbf{F}_g(q_x, \mathbf{q}_\perp, \omega_q + q_x \lambda_k / \gamma_k v_{0,k}) \right]_{\bar{\mathbf{q}}=0}, \quad (47)$$

$$\partial_l \lambda_k = -\frac{i}{g_0(d-2)} \left[\frac{\partial}{\partial q_x} \text{Tr} \mathbf{P}_T(\mathbf{q}) \mathbf{F}_g(q_x, \mathbf{q}_\perp, \omega_q + q_x \lambda_k / \gamma_k v_{0,k}) \right]_{\bar{\mathbf{q}}=0}, \quad (48)$$

$$\partial_l b_k = \frac{1}{v_{0,k}} \frac{1}{d-2} \frac{\partial}{\partial v_{0,k}} [\text{Tr} \mathbf{P}_T(\mathbf{q}) \mathbf{F}_g(q_x, \mathbf{q}_\perp, \omega_q + q_x \lambda_k / \gamma_k v_{0,k})]_{\bar{\mathbf{q}}=0}, \quad (49)$$

$$\partial_l z_k^{(0)} = \frac{1}{v_{0,k}} \frac{1}{2(d-2)} \frac{\partial}{\partial v_{0,k}} \left[\frac{\partial^2}{\partial q_\perp^2} \text{Tr} \mathbf{P}_T(\mathbf{q}) \mathbf{F}_g(q_x, \mathbf{q}_\perp, \omega_q + q_x \lambda_k / \gamma_k v_{0,k}) \right]_{\bar{\mathbf{q}}=0}, \quad (50)$$

$$\partial_l z_k^{(1)} = \frac{1}{v_{0,k}} \frac{1}{2(d-2)} \frac{\partial}{\partial v_{0,k}} \left[\frac{\partial^2}{\partial q_x^2} \text{Tr} \mathbf{P}_T(\mathbf{q}) \mathbf{F}_g(q_x, \mathbf{q}_\perp, \omega_q + q_x \lambda_k / \gamma_k v_{0,k}) \right]_{\bar{\mathbf{q}}=0}, \quad (51)$$

$$\partial_l D_k = -\frac{1}{2(d-2)} [\text{Tr} \mathbf{P}_T(\mathbf{q}) \mathbf{F}_D(q_x, \mathbf{q}_\perp, \omega_q + q_x \lambda_k / \gamma_k v_{0,k})]_{\bar{\mathbf{q}}=0}, \quad (52)$$

where the Galilei transformation mentioned above is implemented on both the external and internal frequencies, ω_q and ω_h , via shifting the argument of the \mathbf{F} 's and a shift in the frequency integration respectively, to ensure comoving fluctuations are captured. Upon rescaling the couplings to dimensionless units,

$$\bar{\kappa}_{0,k} = \frac{\gamma_k \sqrt{\mu_k^\perp \mu_k^x}}{k^{d-2} D_k S^{d-1}} \kappa_{0,k}, \quad \bar{\lambda}_k = \sqrt{\frac{D_k S^{d-1}}{k^{4-d} \gamma_k \mu_k^\perp}} \sqrt{\frac{\mu_k^\perp}{\mu_k^x}} \lambda_k, \quad \bar{b}_k = \frac{D_k S^{d-1}}{k^{4-d} \gamma_k \mu_k^\perp} \sqrt{\frac{\mu_k^\perp}{\mu_k^x}} b_k, \quad (53)$$

$$\bar{z}_k^{(0)} = \frac{D_k S^{d-1}}{k^{2-d} \gamma_k \mu_k^\perp} \sqrt{\frac{\mu_k^\perp}{\mu_k^x}} z_k^{(0)}, \quad \bar{z}_k^{(1)} = \frac{D_k S^{d-1}}{k^{2-d} \gamma_k \mu_k^\perp} \sqrt{\frac{\mu_k^\perp}{\mu_k^x}} z_k^{(1)}, \quad (54)$$

and introducing the anomalous dimensions,

$$\eta_k^\perp = \frac{\partial_l \mu_k^\perp}{\mu_k^\perp}, \quad \eta_k^x = \frac{\partial_l \mu_k^x}{\mu_k^x}, \quad \eta_k^\gamma = \frac{\partial_l \gamma_k}{\gamma_k}, \quad \eta_k^D = \frac{\partial_l D_k}{D_k}, \quad (55)$$

the flow equations take the form,

$$\partial_l \bar{\kappa}_{0,k} = (d-2 + \eta_k^\gamma - \eta_k^D + \frac{1}{2} \eta_k^\perp + \frac{1}{2} \eta_k^x) \bar{\kappa}_{0,k} + f_\kappa, \quad (56)$$

$$\partial_l \bar{\lambda}_k = \frac{1}{2} (4-d + \eta_k^D - \eta_k^\lambda - \frac{5}{2} \eta_k^\perp - \frac{1}{2} \eta_k^x) \bar{\lambda}_k, \quad (57)$$

$$\partial_l \bar{b}_k = (4-d + \eta_k^D - \eta_k^\lambda - \frac{3}{2} \eta_k^\perp - \frac{1}{2} \eta_k^x) \bar{b}_k + f_b, \quad (58)$$

$$\partial_l \bar{z}_k^{(0)} = (2-d + \eta_k^D - \eta_k^\lambda - \frac{3}{2} \eta_k^\perp - \frac{1}{2} \eta_k^x) \bar{z}_k^{(0)} + f_z^{(0)}, \quad (59)$$

$$\partial_l \bar{z}_k^{(1)} = (2-d + \eta_k^D - \eta_k^\lambda - \frac{1}{2} \eta_k^\perp - \frac{3}{2} \eta_k^x) \bar{z}_k^{(1)} + f_z^{(1)}, \quad (60)$$

where,

$$\eta_k^\gamma = 0, \quad (61)$$

$$\eta_k^D = 0, \quad (62)$$

$$\eta_k^\perp = \frac{(d-2)(4-\eta_k^\perp)\Gamma(\frac{6-d}{4})\Gamma(\frac{d}{4})}{16\sqrt{\pi}} \bar{z}_k^{(0)} - \frac{(4-\eta_k^\perp)(1+(5-2d)d)\Gamma(\frac{4-d}{4})\Gamma(\frac{2+d}{4})}{32\sqrt{\pi}(d^2-1)} \bar{\lambda}_k^2, \quad (63)$$

$$\eta_k^x = \frac{(d-2)(4-\eta_k^\perp)\Gamma(\frac{6-d}{4})\Gamma(\frac{d}{4})}{16\sqrt{\pi}} \bar{z}_k^{(1)}, \quad (64)$$

$$f_\kappa = -\frac{(d-2)(4-\eta_k^\perp)\Gamma(\frac{6-d}{4})\Gamma(\frac{d}{4})}{16\sqrt{\pi}}, \quad (65)$$

$$f_b = -\frac{(d-2)(4-\eta_k^\perp)\Gamma(\frac{6-d}{4})\Gamma(\frac{d}{4})}{64\sqrt{\pi}} \bar{b}_k \left(dz_k^{(0)} + 2z_k^{(1)} \right) + \frac{(d-2)(4-\eta_k^\perp)\Gamma(\frac{4-d}{4})\Gamma(\frac{2+d}{4})}{16\sqrt{\pi}} \bar{b}_k^2, \quad (66)$$

$$f_z^{(0)} = -\frac{(4-\eta_k^\perp)}{512(d^2-1)\sqrt{\pi}} \left\{ \left[8(d-2)(d^2-1) \left(d\bar{z}_k^{(0)} + 2\bar{z}_k^{(1)} \right) \bar{z}_k^{(0)} + (6d-d^2)(2d^2-5d-1)\bar{\lambda}_k^2 \bar{b}_k \right] \Gamma\left(\frac{6-d}{4}\right) \Gamma\left(\frac{d}{4}\right) \right. \\ \left. + 4 \left[8(d-2)(d^2-1)\bar{b}_k \bar{z}_k^{(0)} + (2d^2-5d-1) \left((2+d)\bar{z}_k^{(0)} + 2\bar{z}_k^{(1)} \right) \bar{\lambda}_k^2 \right] \Gamma\left(\frac{4-d}{4}\right) \Gamma\left(\frac{2+d}{4}\right) \right\}, \quad (67)$$

$$f_z^{(1)} = -\frac{(d-2)(4-\eta_k^\perp)}{64\sqrt{\pi}} \bar{z}_k^{(1)} \left[\left(d\bar{z}_k^{(0)} + 2\bar{z}_k^{(1)} \right) \Gamma\left(\frac{6-d}{4}\right) \Gamma\left(\frac{d}{4}\right) + 4\bar{b}_k \Gamma\left(\frac{4-d}{4}\right) \Gamma\left(\frac{2+d}{4}\right) \right]. \quad (68)$$

To solve the flow equations, Eq. (63) is first solved algebraically for η_k^\perp and then the flow equations are solved numerically by integrating from different initial conditions. If $\bar{\beta}_k = 0$ and all other couplings nonzero initially, the system is attracted to one of the blue diamonds in Fig. 1a in the MT. For $\lambda_k = 0$ and all other couplings nonzero initially, the system is attracted to the green square in Fig. 1a of the MT and for completely generic couplings the system is attracted to one of the red circles in Fig. 1a of the MT.

The flow diagram, Fig. 1a of the MT, is projected from the 4-dimensional coupling space (after having plugged in the expressions for the η 's, and ignoring $\bar{\kappa}_0$, since all other flow equations no longer depend on it) in the following way: First, since $z_k^{(1)}$ is always attracted towards zero at every fixed point, it is set to zero. Second, $z_k^{(0)}$ is interpolated in such a way, that the location and stability of the fixed points is not impacted, i.e., we set,

$$\bar{z}_k^{(0)} = \bar{z}_k^{(0)*} \frac{\bar{\lambda}_k^2 \bar{b}_k}{\bar{\lambda}_k^{*2} \bar{b}_k^*}, \quad (69)$$

where $\bar{z}_k^{(0)*}$, $\bar{\lambda}_k^*$ and \bar{b}_k^* denote the values of $\bar{z}_k^{(0)}$, $\bar{\lambda}_k$ and \bar{b}_k at the attractive fixed point (red circle in Fig. 1a of the MT), i.e., for $d=3$: $\bar{z}_k^{(0)*} = -1.38$, $\bar{\lambda}_k^* = 7.13$ and $\bar{b}_k^* = 5.73$. Since $\bar{z}_k^{(0)*} = 0$ at all the other fixed points, the locations and stabilities of all fixed points remains unchanged.

In $d=3$ this produces the following two-dimensional set of ordinary differential equations,

$$\partial_t \bar{\lambda}_k = \frac{128\bar{\lambda}_k\sqrt{\pi} - 72\bar{z}_k^{(0)*}\Gamma^2\left(\frac{3}{4}\right) \frac{\bar{\lambda}_k^3 \bar{b}_k}{\bar{\lambda}_k^{*2} \bar{b}_k^*} - 9\Gamma^2\left(\frac{5}{4}\right) \bar{\lambda}_k^3}{256\sqrt{\pi} + 16\bar{z}_k^{(0)*}\Gamma^2\left(\frac{3}{4}\right) \frac{\bar{\lambda}_k^2 \bar{b}_k}{\bar{\lambda}_k^{*2} \bar{b}_k^*} + 2\Gamma^2\left(\frac{5}{4}\right) \bar{\lambda}_k^2}, \quad (70)$$

$$\partial_t \bar{b}_k = \frac{128\sqrt{\pi}\bar{b}_k - 64\Gamma^2\left(\frac{3}{4}\right) \bar{z}_k^{(0)*}\Gamma^2\left(\frac{3}{4}\right) \frac{\bar{\lambda}_k^2 \bar{b}_k^2}{\bar{\lambda}_k^{*2} \bar{b}_k^*} - \Gamma^2\left(\frac{5}{4}\right) (5\bar{\lambda}_k^2 + 32\bar{b}_k)\bar{b}_k}{128\sqrt{\pi} + 8\bar{z}_k^{(0)*}\Gamma^2\left(\frac{3}{4}\right) \frac{\bar{\lambda}_k^2 \bar{b}_k}{\bar{\lambda}_k^{*2} \bar{b}_k^*} + \Gamma^2\left(\frac{5}{4}\right) \bar{\lambda}_k^2}, \quad (71)$$

from which Fig. 1a of the MT is produced. We also produced a flow diagram by simply solving the flow equation for the fixed point solution of $\bar{z}_k^{(0)}$ in terms of $\bar{\lambda}_k$ and \bar{b}_k . While this method seems more elegant on paper, the resulting flow trajectories in the projected two-dimensional plane was much less accurate compared to the method used here. This is probably coincidental.

* p.jentsch20@imperial.ac.uk

[†] c.lee@imperial.ac.uk

- [1] L. Canet, Strong-coupling fixed point of the kardar-parisi-zhang equation (2009), arXiv:cond-mat/0509541 [cond-mat.stat-mech].
- [2] T. R. Morris, Momentum scale expansion of sharp cutoff flow equations, Nuclear Physics B **458**, 477 (1996).